



OPEN

Dielectric properties and Raman spectra of ZnO from a first principles finite-differences/finite-fields approach

Arrigo Calzolari^{1,2} & Marco Buongiorno Nardelli^{2,3}¹Istituto Nanoscienze CNR-NANO-S3, I-41125 Modena, Italy, ²Department of Physics, University of North Texas, Denton, TX 76203, ³Department of Chemistry, University of North Texas, Denton, TX 76203.

Using first principles calculations based on density functional theory and a coupled finite-fields/finite-differences approach, we study the dielectric properties, phonon dispersions and Raman spectra of ZnO, a material whose internal polarization fields require special treatment to correctly reproduce the ground state electronic structure and the coupling with external fields. Our results are in excellent agreement with existing experimental measurements and provide an essential reference for the characterization of crystallinity, composition, piezo- and thermo-electricity of the plethora of ZnO-derived nanostructured materials used in optoelectronics and sensor devices.

ZnO is a wide-band gap, transparent, polar semiconductor with unparalleled optoelectronic, piezoelectric, thermal and transport properties, which make it the material of choice for a wide range of applications such as blue/UV optoelectronics, energy conversion, transparent electronics, spintronic, plasmonic and sensor devices¹. Understanding the infra-red (IR) properties of the bulk crystal is crucial for the intrinsic characterization of the material and is a prerequisite for the viable application of all ZnO-derived systems (e.g. nanostructures, interfaces, alloys) that are now the leading edge of research in many optoelectronic fields. In fact, at IR wavelengths, the vibrational polar modes affect also the dielectric response of the material (i.e. the optical properties), and thus its final performance. This justifies the uninterrupted sequence of experimental reports on vibrational properties of wurtzite ZnO crystal, which started in the sixties and continues nowadays²⁻⁸.

Raman spectroscopy is one of the most common investigation techniques exploited for this purpose because it provides information on the structural and chemical properties such as orientation, crystallinity and existence of defects and impurities. However, despite the profuse research efforts pursued in the last decades, there are still open questions on the unambiguous identification of high-frequency phonon modes or unusual line-width variations⁴ and the interpretation of angular-dependent Raman spectra of ZnO: The uniaxial crystal structure along with the pronounced mass difference and the strong bond polarity imparts a large LO-TO splitting that mixes phonon bands and makes the interaction with external radiation largely anisotropic. Clearly, a unified theoretical approach able to treat at the same level of accuracy both the phonon dispersion and the Raman spectra is highly desirable. Although semiempirical approaches could provide a simple and computationally inexpensive way to treat this problem^{9,10}, the parameterization of the force fields strongly reduces the transferability of the interatomic potentials, which must be carefully tested for each specific system and morphology especially in the presence of doping, defects and impurities. On the other hand, while a few attempts to reproduce ZnO phonon bands through ab initio techniques exist⁷, no simulations of Raman spectra have appeared so far. The challenge resides in the proper treatment of the response of a highly polar material like ZnO to external electric fields.

In principle, Density Functional Perturbation Theory (DFPT)^{11,12} is an elegant and accurate approach for simulation of both phonon and Raman spectra¹⁴. In practice, the required computational effort, and the difficulty in improving the description of the electronic structure beyond the common functional approximations (LDA, PBE, etc.) prevent the application of this techniques for a large class of realistic structures and materials. ZnO is a prototypical example: a standard Density Functional Theory (DFT) description of the band structure of bulk ZnO severely underestimates repetition the band gap ($\Delta E_g^{DFT} = 0.9$ eV vs $\Delta E_g^{\text{exp}} = 3.3$ eV). This is not simply due to the lack of many-body corrections typical of DFT, but rather to an unphysical enhancement of the covalent character of the Zn-O bonds¹⁵. In turn, the wrong description of the electronic structure affects the electrostatic properties of the system and thus the phonon distribution and the coupling with the external fields. This problem

SUBJECT AREAS:
ELECTRONIC STRUCTURE
ELECTRONIC PROPERTIES AND
MATERIALSReceived
5 August 2013Accepted
2 October 2013Published
21 October 2013Correspondence and
requests for materials
should be addressed to
A.C. (arrigo.
calzolari@nano.cnr.it)
or M.B.N. (mbn@unt.
edu)



may be easily overcome by including Hubbard-like corrections¹⁶ or using hybrid functionals¹⁷. However, these features are not readily accessible in DFPT approaches for their large computational cost¹⁸.

In this paper we have solved the problem of simulating with comparable accuracy both the electronic and vibrational spectrum of ZnO using a unified finite-fields/finite-differences approach that is independent of the choice of the functional. This allows us to simulate the phonons, the high and low-frequency dielectric constant and the non-resonant Raman spectra of any material through a finite set of electronic structure and force calculations using the finite displacement method¹⁹.

Results

Unified finite-fields/finite-differences theory. The interatomic Force Constants (IFCs) K and the electronic susceptibility χ are obtained as finite differences of forces and polarizations with respect to atomic displacements or external electric fields²⁰.

IFCs are the second derivatives at equilibrium of the total energy versus the displacements of the ions $u(\mathbf{R})$, or alternatively, the derivative of the atomic forces F versus the ionic displacements:

$$K_{I\alpha, J\beta}(\mathbf{R}-\mathbf{R}') = \frac{\partial^2 E_{tot}}{\partial u_{I\alpha}(\mathbf{R}) \partial u_{J\beta}(\mathbf{R}')} = - \frac{\partial F_{I\alpha}}{\partial u_{J\beta}(\mathbf{R}')}, \quad (1)$$

where \mathbf{R} and \mathbf{R}' are Bravais lattice vectors, I, J are the I -th and J -th atom of the unit cell, and α and β represent the Cartesian components. Phonon frequencies (ω_{ph}) and normal modes ($u_{I\alpha}^m$) are routinely obtained from the resolution of the eigenvalue equation: $\omega_{ph}^2(\mathbf{q}) u_{I\alpha, J\beta}(\mathbf{q}) = \sum_{J\beta} u_{J\beta}(\mathbf{q}) D_{I\alpha, J\beta}(\mathbf{q})$, where the dynamical matrix $D_{I\alpha, J\beta}(\mathbf{q})$ is the Fourier transform of the IFC. The acoustic sum rule (ASR) in real space is defined as in Ref. 12, while long-wavelength dipole-dipole effects are included by means of specific non-analytical correction to the IFCs, as proposed by Yi Wang *et al.*²¹.

The proper treatment of the long wavelength macroscopic polarization field requires also the evaluation of the dielectric tensor and of the Born effective charges. For this purpose we consider the electronic susceptibility:

$$\chi_{ij} = \frac{\partial^2 E_{tot}^{\mathcal{E}}}{\partial \mathcal{E}_i \partial \mathcal{E}_j} = \frac{\partial P_i^{\mathcal{E}}}{\partial \mathcal{E}_j}, \quad (2)$$

where $E_{tot}^{\mathcal{E}}$ is the total energy in the presence of electric field $\mathcal{E}_{i,j}$ and $P^{\mathcal{E}}$ is the electronic polarization along the direction of \mathcal{E} . Here, $E_{tot}^{\mathcal{E}}$ and $P^{\mathcal{E}}$ are evaluated following the method proposed by Umari and Pasquarello²⁰, where the introduction of a non local energy functional $E_{tot}^{\mathcal{E}}[|\psi\rangle] = E^0[|\psi\rangle] - \mathcal{E} \cdot (P^{ion} + P^{el}[|\psi\rangle])$ allows electronic structure calculations for periodic systems under finite homogeneous electric fields. E^0 is the ground state total energy in the absence of external electric fields; P^{ion} is the usual ionic polarization, and P^{el} is given as a Berry phase of the manifold of the occupied bands²².

The high-frequency dielectric tensor ϵ^{∞} is then computed as $\epsilon_{ij}^{\infty} = \delta_{ij} + 4\pi\chi_{ij}$, and the Born effective charge tensor $Z_{i,j}^*$ is defined as the induced polarization along the direction i by a unitary displacement of the I -th atom in the j direction, or alternatively in terms of atomic forces in the presence of the electric field \mathcal{E} :

$$Z_{I,i,j}^* = \frac{\Omega}{e} \frac{\partial P_{I,i}^{\mathcal{E}}}{\partial r_{I,j}} = \frac{\partial^2 E_{tot}^{\mathcal{E}}}{\partial \mathcal{E}_i \partial r_{I,j}} = - \frac{\partial F_{I,i}^{\mathcal{E}}}{\partial \mathcal{E}_j} \quad (3)$$

Finally, the contribution of the polar optical modes to the static dielectric constant $\epsilon^0 = \lim_{\omega \rightarrow 0} \epsilon(\omega)$ is computed using the Lyddane-Sachs-Teller relation^{12,13}: $\epsilon_s^0 / \epsilon_s^{\infty} = \omega_s^2(LO) / \omega_s^2(TO)$ where $\omega(LO)$ ($\omega(TO)$) are the LO (TO) phonon frequencies and s denotes the electric field polarizations parallel (\parallel) and perpendicular (\perp) to the polar axis. This alternative method is implemented and fully integrated in the QUANTUM ESPRESSO suite of codes²³ (www.

quantum-espresso.org; the finite-fields/finite-differences approach is implemented in the package FD in PHonon.).

The calculation of the Raman spectra proceeds along similar lines. The non-resonant Raman intensity for a Stokes process is described by the Placzek's expression²⁴:

$$I \propto \sum_m |\mathbf{e}_i \cdot \alpha^m \cdot \mathbf{e}_s|^2 \frac{(n_m + 1)}{\omega_m}, \quad (4)$$

where \mathbf{e}_i (\mathbf{e}_s) are the polarization of the incident (scattered) radiation, ω_m is the frequency of the generated optical phonon, n_m is the Bose-Einstein distribution, and α_{ij}^m is the Raman tensor, defined as:

$$\alpha_{ij}^m = \sqrt{\Omega} \sum_{I,k} \chi_{ijk}^{(1)} u_{I,k}^m. \quad (5)$$

Within the finite-field approach, the third rank tensor $\chi_{ijk}^{(1)}$ is evaluated in terms of finite differences of atomic forces in the presence of two electric fields²⁵:

$$\chi_{ijk}^{(1)} = \frac{\partial \chi_{ij}}{\partial r_{I,k}} = \frac{\partial^2 P_i^{\mathcal{E}}}{\partial r_{I,k} \partial \mathcal{E}_j} = - \frac{1}{\Omega} \frac{\partial^2 F_{I,k}^{\mathcal{E}}}{\partial \mathcal{E}_i \partial \mathcal{E}_j}. \quad (6)$$

In practice, the tensor $\chi_{ijk}^{(1)}$ is obtained from a set 19 calculations, which combine the finite electric fields $\mathcal{E}_{i,j}$ along the cartesian coordinates. $\chi_{ijk}^{(1)}$ is then symmetrized to recover the full C_{6v} symmetry of the wurtzite structure.

Dielectric and vibrational properties. The calculated high and low frequency dielectric constants, summarized in Table I, are in agreement with experimental spectroscopic ellipsometry data³, as well as Hartree-Fock calculations²⁶. Born effective charges (Table I) are also in agreement with values extracted from transverse IR reflectance spectra²⁷, and may be easily associated to piezoelectric properties of ZnO and its modifications under pressure²⁸.

PBE and PBE + U phonon dispersions are reported in Fig. 1 and phonon frequencies at the Brillouin Zone center (Γ) are summarized in Table II, where we also display the LDA values for comparison. Experimental Inelastic Neutron Scattering (red diamond and blue circles) and Raman (green squares) data are extracted from Ref. 7 and superimposed in Fig. 1 to the first principles data. While LDA and PBE results clearly underestimate the experimental frequencies, mostly in the optical branches, with PBE + U the agreement is very good. Here only the highest-frequency LO bands are slightly overestimated. Notably, these phonon branches suffer of anharmonic renormalization effects, which are not included in the present approach. Furthermore, the error bar on the experimental Raman results is higher for these bands, due to the low cross-section of the corresponding phonon-photon scattering processes (see below).

Following the irreducible representation of the wurtzite symmetry group C_{6v} , the phonon modes of ZnO can be classified as $\Gamma = 2A_1 + 2B_1 + 2E_1 + 2E_2$. One low energy A_1 and one double E_1 modes correspond to the transverse and longitudinal acoustic branches, the others are optical modes. B_1 modes are IR and Raman inactive. The two E_2 modes are non polar IR inactive but Raman active. In A_1

Table I | High-frequency (ϵ^{∞}) and static (ϵ^0) dielectric constant and effective Born charges (Z^*) of wurtzite ZnO, for electric field polarization parallel and perpendicular to the c-axis. Corresponding experimental values are reported in parenthesis

| | ϵ^{∞} | ϵ^0 | Z^* |
|--------------------------|--------------------------|--------------------------|--------------------------|
| $\mathcal{E}(\parallel)$ | 3.14 (3.78) ^a | 7.76 (8.91) ^a | 2.12 |
| $\mathcal{E}(\perp)$ | 3.08 (3.70) ^a | 6.98 (7.77) ^a | 2.06 (2.02) ^b |

^afrom Ref. 3.
^bfrom Ref. 27.

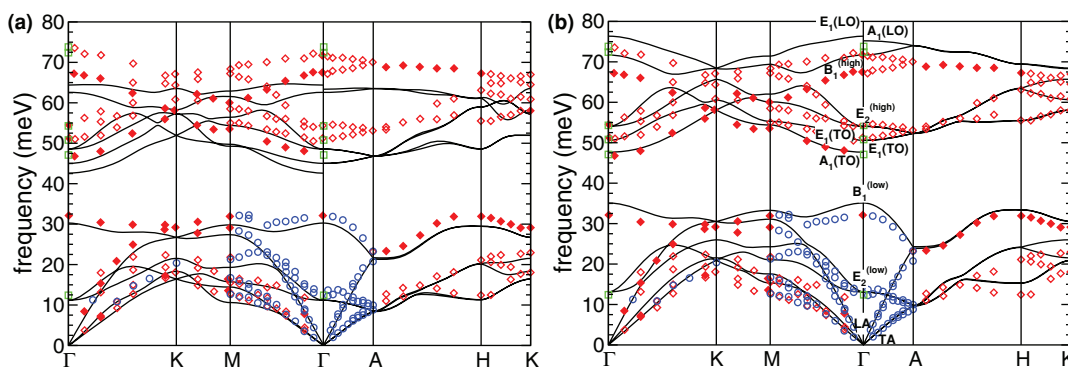


Figure 1 | Calculated (black lines) phonon dispersions for wurtzite ZnO calculated with (a) PBE and (b) PBE + U. Solid/open diamonds (red) and open circles (blue) represent experimental INS data, green squares represent Raman frequencies. Experimental data reproduced from Ref. 7.

and E_1 polar modes, atoms move parallel and perpendicular to the c -axis respectively and are the ones responsible for the LO-TO splitting. The labeling in Fig. 1 and Table II is based on the direct analysis of the phonon eigenmodes and their underlying symmetry. Note that PBE calculations give an incorrect ordering of the B_1 and $A_1(\text{LO})$ modes that is instead correct in PBE + U (see Table II).

Raman spectroscopy. We calculated the Raman spectra for different propagation (\mathbf{k}) and polarization ($\mathbf{e}_{i,s}$) directions of the incoming and scattering light, as shown in Fig. 2. We simulated the Raman spectra for different rotation angles (θ) of the polarization vectors in the planes parallel (a-plane) and perpendicular (c-plane) to the c -axis. Following the standard experimental setups, for c -plane spectra we considered only parallel polarization of the incoming and scattered light [$z(\text{xx})\bar{z} \leftrightarrow z(\text{yy})\bar{z}$]. We used the Porto notation: symbols inside the parentheses indicate the direction of \mathbf{e}_i and \mathbf{e}_s , while symbols outside the parentheses indicate the directions of propagation of light (\mathbf{k}). In the a-plane case, two different orientations of $\mathbf{e}_{i,s}$ can be experimentally detected: $y(\text{xx})\bar{y} \leftrightarrow y(\text{zz})\bar{y}(\mathbf{e}_i \parallel \mathbf{e}_s)$ and $y(\text{xz})\bar{y} \leftrightarrow y(\text{zx})\bar{y}(\mathbf{e}_i \perp \mathbf{e}_s)$.

Results for room temperature boson distribution are summarized in Fig. 2. Panel (a) shows the a-plane spectra for parallel polarization vector configurations, which reproduces the angular modification of experimental spectra^{3,8} and the reciprocal intensity ratio of the main peaks. The spectra are, in fact, dominated by Stokes processes due to the $A_1(\text{TO})$ and $E_2^{(\text{high})}$ phonon modes at 384 and 436 cm^{-1} , respectively, only 2 cm^{-1} from the experimental values. The intensity of the $A_1(\text{TO})$ peak is independent from the orientation of incident polarization, while the $E_2^{(\text{high})}$ peak reaches a maximum at 90° and minima at 0° and 180° . For 20° , 40° , 120° , and 140° a small contribution from $E_1(\text{TO})$ also appears at 410 cm^{-1} . The $E_1^{(\text{high})}$ phonon mode at

106 cm^{-1} is not visible in this energy scale, the LO modes are not allowed by symmetry for this incident light direction.

Similar arguments apply for the a-plane spectra for $\mathbf{e}_i \perp \mathbf{e}_s$ polarizations, as displayed in panel (b). Here the main contributions stem from the $E_1(\text{TO})$ and $E_2^{(\text{high})}$ modes, whose reciprocal intensity depends on the θ angle. The two peaks are in counter phase: the former has maxima at 0° , 90° and 180° , where the latter reaches the minimum, and vice versa. Besides these two peaks, experimental results for crossed polarization vectors exhibit small, angular-dependent features associated to $A_1(\text{TO})$ and $E_1(\text{LO})$ that should be symmetry forbidden in this geometry. This is indeed a consequence of the deviation from the ideal geometry set-up and/or a deviation from perfect hexagonal crystallinity of the sample. Following Ref. 8 we considered non-orthogonal polarization vectors,

$$\mathbf{e}_i = \frac{1}{\sqrt{1+p^2}} \begin{pmatrix} \cos\theta \\ p \\ \sin\theta \end{pmatrix}, \quad \mathbf{e}_s = \frac{1}{\sqrt{1+p^2}} \begin{pmatrix} -\sin\theta \\ p \\ \cos\theta \end{pmatrix}, \quad (7)$$

through the inclusion of an arbitrary constant p . The angular distribution and intensity of the peaks depend on the choice of the p factor, i.e. on the characteristic crystallinity of the sample. Results for $p = 0.5$ are reported in the inset of panel (b) where the $A_1(\text{TO})$ peak and a small contribution from $E_1(\text{LO})$ appear.

From the spectra of Fig. 2 we can also extract the relative intensity ratio between the main Stokes peaks, which are univocally related to the non-zero matrix elements of the Raman tensor for the C_{6v} point group (see for instance Ref. 29). Calculated ratios between A_1 (E_1) and $E_2^{(\text{high})}$, taken as reference, are 0.54 and 0.23, respectively; the corresponding experimental values are 0.6 and 0.4⁸. The agreement is quite satisfactory for A_1 , while it is slightly worse for E_1 . However, in the latter case the experimental value is extracted from $\mathbf{e}_i \perp \mathbf{e}_s$ polarizations spectra, which may suffer of non-ideal hexagonal symmetry, as discussed above (Fig. 2b).

Table II | Phonon frequencies (in cm^{-1}) of ZnO at Brillouin Zone center (Γ), calculated with LDA, PBE, PBE + U and compared to experimental Raman data from Ref. 7

| Mode (Γ) | LDA | PBE | PBE + U | Exp (Raman) |
|-----------------------|-----|-----|---------|-------------|
| TA/TA | 0 | 0 | 0 | 0 |
| $E_w^{(\text{low})}$ | 87 | 89 | 106 | 100 |
| $B_1^{(\text{low})}$ | 258 | 243 | 283 | - |
| $A_1(\text{TO})$ | 398 | 343 | 384 | 380 |
| $E_1(\text{TO})$ | 420 | 363 | 408 | 410 |
| $E_2^{(\text{high})}$ | 446 | 392 | 436 | 438 |
| $B_1^{(\text{high})}$ | 539 | 505 | 578 | - |
| $A_1(\text{LO})$ | 547 | 498 | 607 | (584) |
| $E_1(\text{LO})$ | 560 | 508 | 615 | (595) |

Discussion

Our results demonstrate that the coupled finite-fields/finite-differences DFT approach is essential to accurately evaluate the dielectric properties, phonon dispersions and Raman spectra of ZnO. By reducing high order derivatives of the total energy (i.e. of the charge density) to lower order differences of polarizations and forces obtained from a limited set of self-consistent DFT simulations, it favors the inclusion of advanced corrections to the ground-state electronic structure that are essential for the proper description of the system. In particular, the ground state electronic structure and the coupling with external fields in ZnO require the use of *ad hoc* corrections to the position of the d-bands of Zn that can be achieved with a DFT + U treatment, as summarized in Fig. 3. In the case of

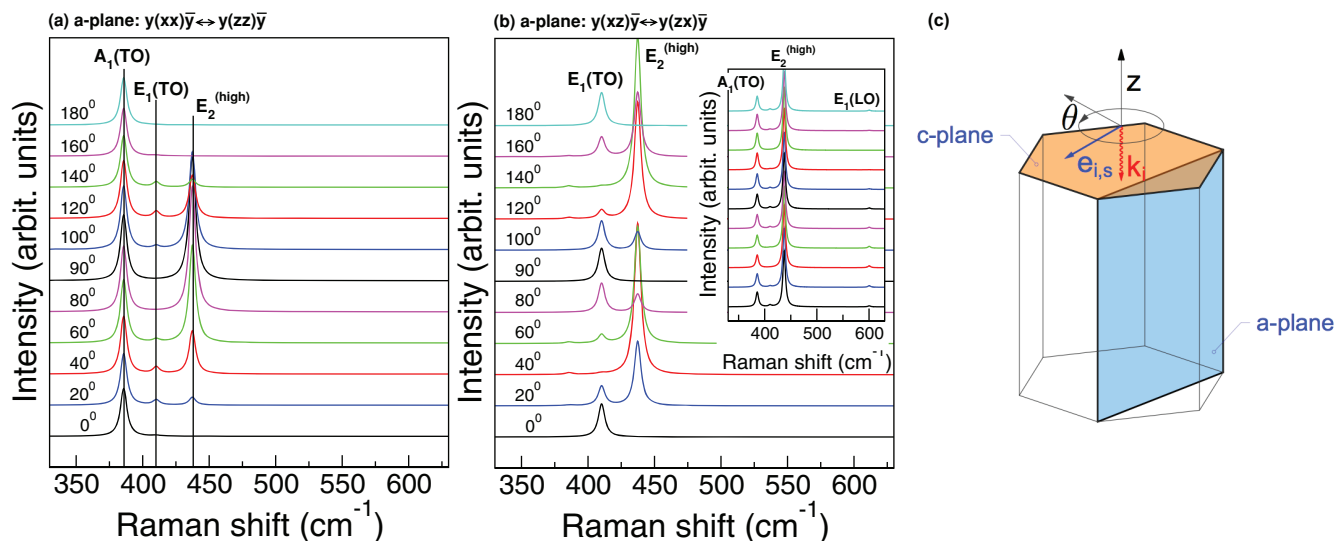


Figure 2 | Calculated Raman spectra for different rotation angles on the a-plane in the parallel (a) and perpendicular polarization vector configurations. The inset of panel (b) shows the modification of the spectrum upon relaxation of the ideal scattering geometry. (c) Scheme of the wurtzite lattice and high symmetry planes perpendicular (c-plane) and parallel (a-plane) to the polar (0001) c-axis. \mathbf{k}_i indicates the propagation direction of light, $\mathbf{e}_{i,s}$ are the incident and scattered polarization vectors; θ is the rotation angle in the plane perpendicular to the \mathbf{k}_i direction.

standard LDA and PBE calculations we observe a severe underestimation of the bandgap (E_{gap}) and a wrong energy position of the d-bands of the Zn atoms, that in turn give an inadequate description of the phonon dispersions (see Fig. 1(b) and discussion therein). The choice of functional influences directly the electrostatics and thus also the characteristics of the vibrational response of the system. In fact, the IFCs are the sum of two contributions:

$$K_{zi,\beta j}(\mathbf{R}-\mathbf{R}') = K_{zi,\beta j}^{el}(\mathbf{R}-\mathbf{R}') + K_{zi,\beta j}^{ion}(\mathbf{R}-\mathbf{R}') \quad (8)$$

where $K_{zi,\beta j}^{ion}$ are the second derivatives of Ewald sums corresponding to the ion-ion repulsion potential, while the electronic contributions $K_{zi,\beta j}^{el}$ are the second derivatives of the electron-electron and

electron-ion terms in the ground state energy. It is the last term that reflects directly in the vibrational spectrum the wrong position of the d-states and the dramatic underestimation of the gap. On the other hand, LDA, with its overestimation of the bonding (shorter lattice parameter and stiffer IFCs) accidentally gives results that are marginally closer to the experimental data thanks to a fortuitous cancellation of errors. The inclusion of the Hubbard U, by correcting the d-Zn p-O hybridization, properly describes not only the electronic bands but also the vibrational and dielectric properties in agreement with the experimental results¹⁵. Notably, the values of the dielectric constants obtained with LDA ($\epsilon_{\parallel} = 5.37$, $\epsilon_{\perp} = 5.39$) and PBE ($\epsilon_{\parallel} = 5.24$, $\epsilon_{\perp} = 4.97$) are much higher than in experiments, a clear indication of a lesser polarity of the system in these approximations.

Finally, the finite-fields/finite-differences framework allows straightforward developments of the theory to include 3rd order terms in the IFCs (i.e. anharmonic contribution to phonons) or susceptibility $\chi^{(2)}$ for the simulation of non-linear optical properties such as hyper-Raman or electro-optic effects. One example of the latter is the Raman signal along the parallel c-plane $z(xx)\bar{z} \leftrightarrow z(yy)\bar{z}$, shown in Fig. 4, where the $A_1(\text{LO})$ and $E_2^{(\text{high})}$ modes dominate the spectrum for all angles (0–180°) (black solid line). However, although allowed by symmetry, $A_1(\text{LO})$ is invisible or hardly visible in most experimental data collections^{2,3,6,8}. This effect is due to a competitive interaction with the Fröhlich term², which couples with the macroscopic field generated by the $A_1(\text{LO})$ mode and cancels most of the deformation potential contributions. This effect may be evaluated including a non-linear correction to the tensor $\chi_{ijl}^{(1)}$ for the longitudinal q_l mode³⁰

$$\frac{\partial \chi_{ij}}{\partial r_{l,k}} = \frac{\partial \chi_{ij}}{\partial r_{l,k}} \Big|_{\epsilon=0} - \frac{8\pi \sum_l Z_{l,kl}^* q_l}{\Omega \sum_l q_l \epsilon_{ll}^{\infty} q_l} \sum_l \chi_{ijl}^{(2)} q_l, \quad (9)$$

where the third order tensor $\chi_{ijl}^{(2)}$ may be straightforwardly calculated extending the finite field approach to the case of three electric fields, or alternatively:

$$\chi_{ijl}^{(2)} = \frac{\partial^3 E_{tot}}{\partial \mathcal{E}_i \partial \mathcal{E}_j \partial \mathcal{E}_l} = \frac{1}{4\pi} \frac{\partial \epsilon_{ij}^{\mathcal{E}}}{\partial \mathcal{E}_l} \quad (10)$$

Indeed, the inclusion of the Fröhlich term suppresses the $A_1(\text{LO})$ (red dashed line) in agreement with experiments.

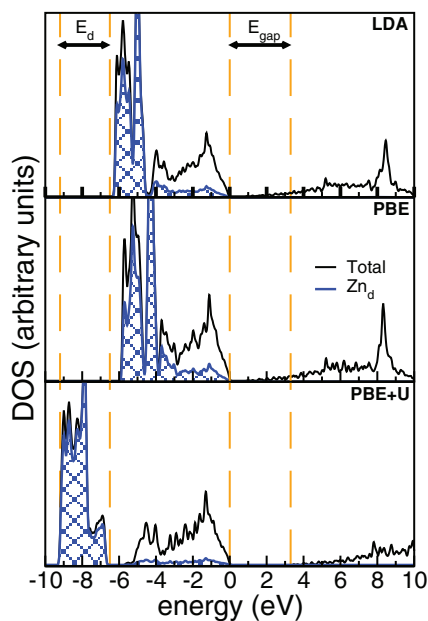


Figure 3 | Density of states of hexagonal ZnO crystal with LDA, PBE and PBE + U (from top to bottom). Energies are referred to the respective top of valence bands. The vertical lines indicate the experimental energy gap (E_{gap}) and 3d-band width (E_d) from Ref. 15.

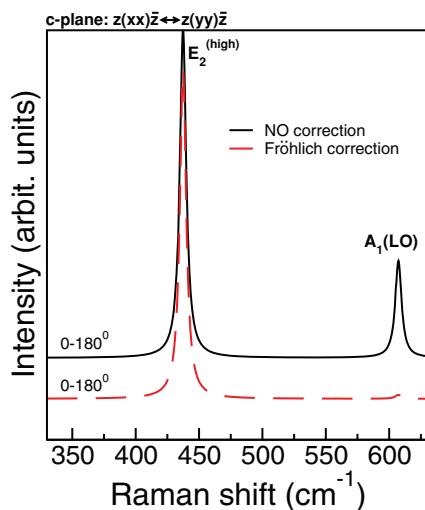


Figure 4 | Calculated Raman spectra of c-plane sample in the parallel polarization vector configuration with (red) and without (black) Fröhlich correction to longitudinal optical phonons.

In conclusion, we have demonstrated that our unified finite-fields/finite-differences technique provides a general framework for the calculation of the vibrational, dielectric and Raman properties of materials, without any limitation in the choice of the DFT framework. We have applied this method to the study of ZnO, a material that for its complex electronic structure requires a special treatment in order to obtain a faithful representation of its properties. Our results are in excellent agreement with available experimental data.

Methods

Computational details. We calculated vibrational and Raman spectra of wurtzite ZnO bulk using PBE-GGA³¹ ultrasoft pseudopotentials³² for all the atomic species, a 28 (280) Ry energy cut off in the plane wave expansion of wavefunctions (charge) and a $(12 \times 12 \times 8)$ regular k-point mesh. LDA calculations have been done with norm-conserving Troullier-Martins pseudopotentials³³, with a kinetic energy cutoff of 100 Ry. *3d* electrons of Zn have been explicitly included in the valence for both cases. For PBE + U, a Hubbard-like potential with $U = 12.0$ eV and $U = 6.5$ eV is applied on the *3d* orbitals of zinc and on the *2p* orbitals of oxygen, respectively¹⁶. Note that the Hubbard U values included in the calculations do not have to be considered as physical on-site electron-electron screened potentials, in the sense of the many-body Hubbard Hamiltonian, but as empirical parameters introduced to correct the gap. This is an efficient and computationally inexpensive way to correct for the severe underestimation of the bandgap and the wrong energy position of the d-bands of the Zn atoms^{15,34}. This procedure has also been applied to other similar systems^{35–38}. D_{ext} and α^m are obtained applying $\mathcal{E} = 0.003$ a.u. along the cartesian axes. All calculations have been run with lattice parameters optimized for each functional¹⁶.

For the calculation of phonon modes we considered a $(8 \times 8 \times 2)$ hexagonal supercell (512 atoms) and we calculated forces (i.e. IFC) displacing only 2 atoms in primitive ZnO cell along the two inequivalent directions. This corresponds to a set of 4 DFT calculations. The Raman tensor has been calculated on the primitive wurtzite cell.

- Morkoç, H. & Özgür, Ü. *Zinc Oxide: Fundamentals, Materials and Device Technology* (Wiley-VCH Verlag GmbH and Co. KGaA, Weinheim, 2009).
- Callender, R., Sussman, S., Seldes, M. & Chang, R. Pressure dependence of the lattice dynamics of ZnO: an ab initio approach. *Phys. Rev. B* **7**, 3788 (1973).
- Ashkenov, N. *et al.* Infrared dielectric functions and phonon modes of high quality ZnO films. *J. Appl. Phys.* **93**, 126 (2003).
- Serrano, J. *et al.* Dispersive phonon linewidths: the E2 phonon of ZnO. *Phys. Rev. Lett.* **90**, 055510 (2003).
- Bergman, L., Chen, X.-B., Huso, J., Morrison, J. L. & Hoecck, H. Raman scattering of polar modes of ZnO crystallites. *J. Appl. Phys.* **98**, 093507 (2005).
- Cusco, R. *et al.* Temperature dependence of Raman scattering in ZnO. *Phys. Rev. B* **75**, 165202 (2007).
- Serrano, J. *et al.* Phonon dispersion relations of zinc oxide: inelastic neutron scattering and ab initio calculations. *Phys. Rev. B* **81**, 174304 (2010).
- Sander, T., Eisermann, S., Meier, B. K. & Klar, P. J. Raman tensor elements of wurtzite ZnO. *Phys. Rev. B* **85**, 165208 (2012).
- Richard, C. *et al.* Zinc Oxide: A Case Study in Contemporary Computational Solid State Chemistry. *J. Comp. Chem.* **29**, 2234–2249 (2009).

- Gale, J. D. & Rohl, A. L. The General Utility Lattice Program (GULP). *Mol. Sim.* **29**, 291–341 (2003).
- Baroni, S., De Gironcoli, S., Dal Corso, A. & Giannozzi, P. Phonons and related crystal properties from density-functional perturbation theory. *Rev. Mod. Phys.* **73**, 515–562 (2001).
- Gonze, X. & Lee, C. Dynamical matrices, Born effective charges, dielectric permittivity tensors, and interatomic force constants from density-functional perturbation theory. *Phys. Rev. B* **55**, 10355–10368 (1997).
- Cochran, W. & Cowley, R. A. Dielectric constants and lattice vibrations. *J. Phys. Chem. Sol.* **23**, 447–450 (1962).
- Lazzeri, M. & Mauri, F. First-Principles Calculation of Vibrational Raman Spectra in Large Systems: Signature of Small Rings in Crystalline SiO₂. *Phys. Rev. Lett.* **90**, 036401 (2003).
- Vogel, D., Kruger, P. & Pollmann, J. Self-interaction and relaxation-corrected pseudopotentials for II-VI semiconductors. *Phys. Rev. B* **54**, 5495–5511 (1996).
- Calzolari, A., Ruini, A. & Catellani, A. Anchor group versus conjugation: towards the gap-state engineering of functionalized ZnO(10-10) surface for optoelectronic applications. *J. Am. Chem. Soc.* **133**, 5893 (2011).
- Labat, F., Ciofini, I. & Adamo, C. Modeling ZnO phases using a periodic approach: From bulk to surface and beyond. *J. Chem. Phys.* **131**, 044708 (2009).
- Floris, A., de Gironcoli, S., Gross, E. K. U. & Cococcioni, M. Vibrational properties of MnO and NiO from DFT + U-based density functional perturbation theory. *Phys. Rev. B* **84**, 161102R (2011).
- Leibfried, G. & Ludwig, W. *Solid State Physics*. ed. by Seitz, F. and Turnbull, D. vol. **12**, p. 275, (Academic Press, NY, 1961).
- Umari, P. & Pasquarello, A. Ab initio molecular dynamics in a finite homogeneous electric field. *Phys. Rev. Lett.* **89**, 157602 (2002).
- Wang, Y., Shang, S., Liu, Z.-K. & Chen, L.-Q. Mixed-space approach for calculation of vibration-induced dipole-dipole interactions. *Phys. Rev. B* **85**, 224303 (2012).
- King-Smith, R. & Vanderbilt, D. Theory of polarization of crystalline solids. *Phys. Rev. B* **47**, 1651–1654 (1993).
- Giannozzi, P. *et al.* QUANTUM ESPRESSO: a modular and open-source software project for quantum simulations of materials.: *J. Phys. Cond. Matt.* **21**, 395502 (2009).
- Bruesch, P. in Fulde, P. *Phonons: theory and experiments II* (Springer-Verlag, Berlin 1986).
- Umari, P., Gonze, X. & Pasquarello, A. Concentration of Small Ring Structures in Vitreous Silica from a First-Principles Analysis of the Raman Spectrum. *Phys. Rev. Lett.* **90**, 027401 (2003).
- Noel, Y., Zicovich-Wilson, C. M., Civalleri, B., DARco, P. & Dovesi, R. Polarization properties of ZnO and BeO: An ab initio study through the Berry phase and Wannier functions approaches. *Phys. Rev. B* **65**, 014111 (2001).
- Decremps, F., Pellicer-Porres, J., Saitta, A. M., Chervin, J.-C. & Polian, A. High-pressure Raman spectroscopy study of wurtzite ZnO. *Phys. Rev. B* **65**, 092101 (2001).
- Klingshirn, C. *Semiconductor Optics* 3rd Ed. (Springer-Verlag, Berlin, 2007).
- Cardona, M. *Light scattering in solids II* Cardona, M. & Güntherodt, G. (ed.) (Springer-Verlag, Berlin, 1982).
- Veithen, M., Gonze, X. & Ghosez, P. Non linear optical susceptibility, Raman efficiencies, and electro-optic tensors from first-principles density functional perturbation theory. *Phys. Rev. B* **71**, 125107 (2005).
- Perdew, J. P., Burke, K. & Ernzerhof, M. Generalized Gradient Approximation Made Simple. *Phys. Rev. Lett.* **77**, 3865–3868 (1996).
- Vanderbilt, D. Soft self-consistent pseudopotentials in a generalized eigenvalue formalism. *Phys. Rev. B* **41**, R7892–R7895 (1990).
- Troullier, N. & Martins, J. L. Efficient pseudopotentials for plane-wave calculations. *Phys. Rev. B* **43**, 1993–2006 (1991).
- Janotti, A., Segev, D. & Van de Walle, C. G. Effects of cation d states on the structural and electronic properties of III-nitride and II-oxide wide-band-gap semiconductors. *Phys. Rev. B* **74**, 045202 (2006).
- Dong, Y. & Brillson, L. First-Principles Studies of Metal (111)/ZnO0001 Interfaces. *J. Electron. Mater.* **37**, 743–748 (2008).
- D'Amico, N. R., Cantele, G. & Ninno, D. First-Principles Calculations of clean and defected ZnO surface. *J. Phys. Chem. C* **116**, 21391–21400 (2012).
- Caddeo, C., Mallocci, G., Rignanese, G., Colombo, L. & Mattoni, A. Electronic properties of hybrid ZnO-Oligothiophene nanostructures. *J. Phys. Chem. C* **116**, 8174–8180 (2012).
- Terentjevs, A., Catellani, A., Prendergast, D. & Cicero, G. Importance of on-site corrections to the electronic and structural properties of InN in crystalline solid, nonpolar surface, and nanowire forms. *Phys. Rev. B* **82**, 165307 (2010).

Acknowledgments

We would like to thank Michele Lazzeri, Paolo Umari and Marco Fornari for support and useful discussions, and Rosa Di Felice for a critical reading of the manuscript. Rita Stacchezzini provided valuable graphical aid. This work was supported, in part, by SRC through Task ID P14924 in the Center for Electronic Materials Processing and Integration at the University of North Texas, and ONR-MURI N000141310635. Computational resources have been provided by the UNT HPC Initiative and the Texas Advanced Computing Center (TACC) of the University of Texas, Austin.



Author contributions

A.C. and M.B.N. designed the research, performed the calculations, analyzed the data and co-wrote the paper. M.B.N. wrote the finite-difference codes for phonon calculations. A.C. wrote the code for the finite-field calculation of the Raman tensor.

Additional information

Competing financial interests: The authors declare no competing financial interests.

How to cite this article: Calzolari, A. & Buongiorno Nardelli, M. Dielectric properties and Raman spectra of ZnO from a first principles finite-differences/finite-fields approach. *Sci. Rep.* **3**, 2999; DOI:10.1038/srep02999 (2013).



This work is licensed under a Creative Commons Attribution-NonCommercial-NoDerivs 3.0 Unported license. To view a copy of this license, visit <http://creativecommons.org/licenses/by-nc-nd/3.0>